ACS OMEGA

http://pubs.acs.org/journal/acsodf

Article

# Surface Oxygen Vacancies of Rutile Nanorods Accelerate Biomineralization

Yanwen Yu, Tong Wu,* and Lingqing Dong

Cite This: *ACS Omega* 2023, 8, 20066−20072

Read Online

ACCESS | Metrics & More | Article Recommendations

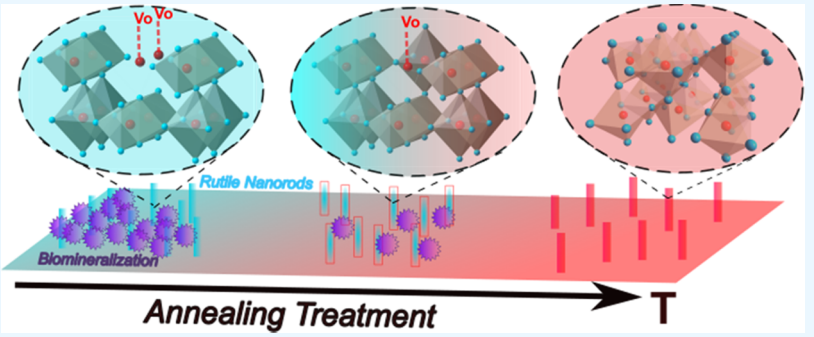


**ABSTRACT:** Titanium dioxide ($TiO_2$) materials have been widely used in biomedical applications of bone tissue engineering. However, the mechanism underlying the induced biomineralization onto the $TiO_2$ surface still remains elusive. In this study, we demonstrated that the surface oxygen vacancy defects of rutile nanorods could be gradually eliminated by the regularly used annealing treatment, which restrained the heterogeneous nucleation of hydroxyapatite (HA) onto rutile nanorods in simulated body fluids (SBFs). Moreover, we also observed that the surface oxygen vacancies upregulated the mineralization of human mesenchymal stromal cells (hMSCs) on rutile $TiO_2$ nanorod substrates. This work therefore emphasized the importance of subtle changes of surface oxygen vacancy defective features of oxidic biomaterials during the regularly used annealing treatment on their bioactive performances and provided new insights into the fundamental understanding of interactions of materials with the biological environment.

## 1. INTRODUCTION

Titanium dioxide ($TiO_2$) nanomaterials have been considered one of the promising biomaterials owing to their good biocompatibility, chemical stability, and mechanical properties.[1] Several decades ago, Prof. Kokubo found that $TiO_2$ was an ideal biomaterial for bone tissue engineering because of its highly induced biomineralization capacity, facilitating the heterogeneous nucleation of HA.[2] Thereafter, various strategies, such as topography design,[3] composite control,[4] surface group modification,[5] etc., have been proposed to fabricate $TiO_2$-based biomaterials. However, the mechanism underlying the induced biomineralization onto the $TiO_2$ surface still remains an open question.

Thermodynamically, the heterogeneous nucleation of apatite onto the material surface is to minimize the interfacial energy via attracting molecules or ions in solution, which is naturally dependent on the surface atomic structure of the material surface.[6−8] For instance, Lu et al. suggested that loosely bonded hydroxyl groups and water on the rutile surface enhanced $Ca^{2+}$ adsorption, which might be the reason for the induced HA formation on alkali-treated Ti surfaces in simulated body fluids (SBFs).[9] Meanwhile, oxygen vacancies, as the most prevalent defects in many oxides, are sensitive to the preparation processing.[10,11] Therefore, we hypothesize that manipulation of surface oxygen vacancies might provide a tool to control the biomineralization process on $TiO_2$.

Recently, we have reported that the surface oxygen vacancy defects of rutile nanorods are able to simultaneously accelerate osteogenesis and angiogenesis.[12] However, these previous efforts have only reported the method of redox processing to control the concentration of surface oxygen vacancy defects of rutile nanorods. Actually, the annealing treatments are more regularly used during oxidic biomaterial preparation. Nevertheless, little attention has been paid to notice the subtle changes of surface oxygen vacancy defective features during the annealing treatments. Moreover, significant scope of the effects

Received: April 7, 2023
Accepted: May 16, 2023
Published: May 25, 2023





https://doi.org/10.1021/acsomega.3c02348
*ACS Omega* 2023, 8, 20066−20072

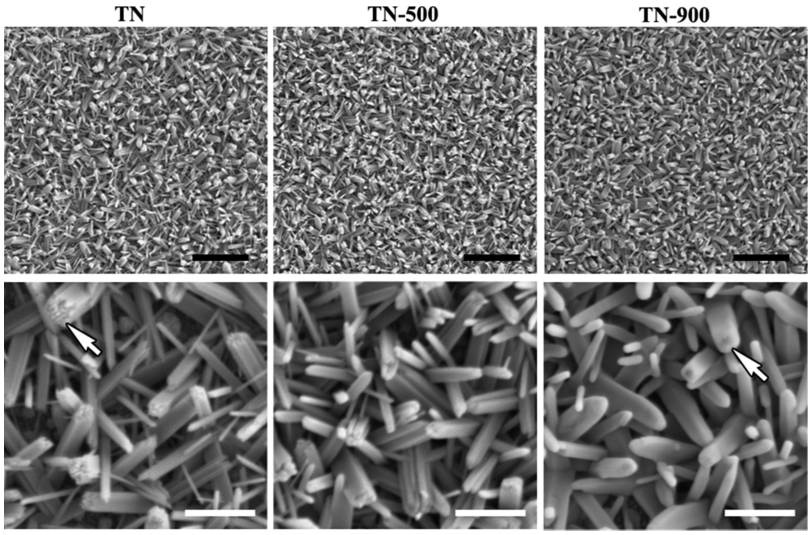


**Figure 1.** SEM images of the three groups of rutile $TiO_2$ nanorod substrates with low (upper) and high (lower) magnification. Scale bars with black and white colors are 2 $\mu$m and 500 nm, respectively. The white arrows in lower images indicate the typical head topography of the rutile $TiO_2$ nanorod.

of surface oxygen vacancy defects on biomineralization still remains to be uncovered.

In this study, we demonstrated that the surface oxygen vacancy defects of rutile nanorods could be gradually eliminated by the regularly used annealing treatment, which restrained the heterogeneous nucleation of hydroxyapatite (HA) onto rutile nanorods in SBF. Moreover, we also observed that the surface oxygen vacancies upregulated the mineralization of hMSCs on rutile $TiO_2$ nanorod substrates.

## 2. EXPERIMENTAL SECTION

**2.1. Preparation and Characterization of Rutile $TiO_2$ Nanorod Films.** The rutile $TiO_2$ nanorod film on quartz substrates was prepared using the two-step method as reported previously.[13] First, the spinning coating method at 6000 rpm for 20 s was used to prepare a $TiO_2$ nanodot film on the quartz substrates (1 cm × 1 cm) as the crystal seeds. The spinning solution was an ethanol solution with acetylacetone (AcAc)/tetrabutyl titanate (TBOT)/$H_2O$ (0.3:1:1 by molar ratio), as well as 40 mg/L polyvinyl pyrrolidone (PVP). Then, the $TiO_2$ nanodot film was annealed in air atmosphere at 500 °C for 1 h. Second, the hydrothermal growth of $TiO_2$ nanorods at 160 °C for 2 h was carried out. The hydrothermal solution was 19 wt % hydrochloric acid solution with 0.42 ml of TBOT in a 100 mL Teflon-lined stainless steel autoclave. After the reaction, the rutile $TiO_2$ nanorod film on quartz substrates was obtained. The annealing treatment of the rutile $TiO_2$ nanorod film (TN) was carried out at 500 °C (TN-500) and 900 °C (TN-900) for 1 h in air atmosphere.

The morphology of the $TiO_2$ nanorod film was observed by field-emission scanning electron microscopy (FESEM, SU-70, Hitachi). The X-ray powder diffraction patterns were measured on an X-ray diffractometer (X-pert Powder, the Netherlands) using Cu K$\alpha$ radiation at a wavelength of 1.54056 Å. The microstructure and the surface atomic structure of rutile $TiO_2$ nanorods were further observed by a transmission electron microscope (TEM, Philips Tecnai F20) and a spherical aberration (Cs) corrected TEM (Titan ChemiSTEM). The surface oxygen vacancies of rutile $TiO_2$ nanorods were further evaluated by X-ray photoelectron spectroscopy (XPS, Thermo Scientific ESCALAB 250Xi) with an Al K$\alpha$ source (1486.6 eV). All binding energies were referenced to the carbon 1s component (284.6 eV).

**2.2. Biomineralization on Rutile $TiO_2$ Nanorods in Simulated Body Fluid (SBF).** The biomineralization capacity of rutile $TiO_2$ nanorods was evaluated by using the SBF solution. Briefly, the rutile $TiO_2$ nanorod films on quartz substrates were immersed in a sealing modified simulated body fluid (1820, PHYGENE) solution at 37 °C for 7 days. The substrates were kept upside down to avoid the deposition of minerals on the surface caused by gravity. Finally, the substrates were washed using water three times and allowed to dry in ambient air.

**2.3. Biomineralization of Mesenchymal Stem Cells (MSCs) on Rutile $TiO_2$ Nanorods.** Human mesenchymal stem cells (hMSCs) were used as the model cells. They were kindly provided by Dr. Ying Zhou of Stomatology Hospital, School of Stomatology, Zhejiang University School of Medicine.[14] Human bone marrow was collected from iliac crest bone aspirates of healthy donors with the approval from The Ethics Committee of First Affiliated Hospital of Medical College, Zhejiang University, as well as the informed consent given by the donors (reference number 2016294). Briefly, the marrow was stored in a 15 mL centrifugal tube cooled by ice. The hMSCs were isolated by Histopaque-1077 (Sigma-Aldrich, St. Louis, MO) and density-gradient centrifugation. They were cultured in a growth medium containing $\alpha$-MEM (Gibco) and 10% fetal bovine serum (FBS, Gibco) at 37 °C in a humid atmosphere with 5% $CO_2$. Typically, the hMSCs were seeded on the substrates placed in 24-well plates using a density of $4 \times 10^4$ cells/well. After culturing for 11 days, the substrates were fixed by 70% ethanol and incubated with Alizarin Red S in an ammonium hydroxide/water solution (w/v 1%) for 20 min. The calcium deposition of different substrates was imaged using a Canon EOS 750D. For the quantitative analysis, the stained substrates were incubated in 10% cetylpyridinium chloride (10 mmol/L dd$H_2O$ supplemented with sodium orthophosphate) for 15 min. Then, the absorbance of the supernatant after extraction was then


https://doi.org/10.1021/acsomega.3c02348
ACS Omega 2023, 8, 20066−20072

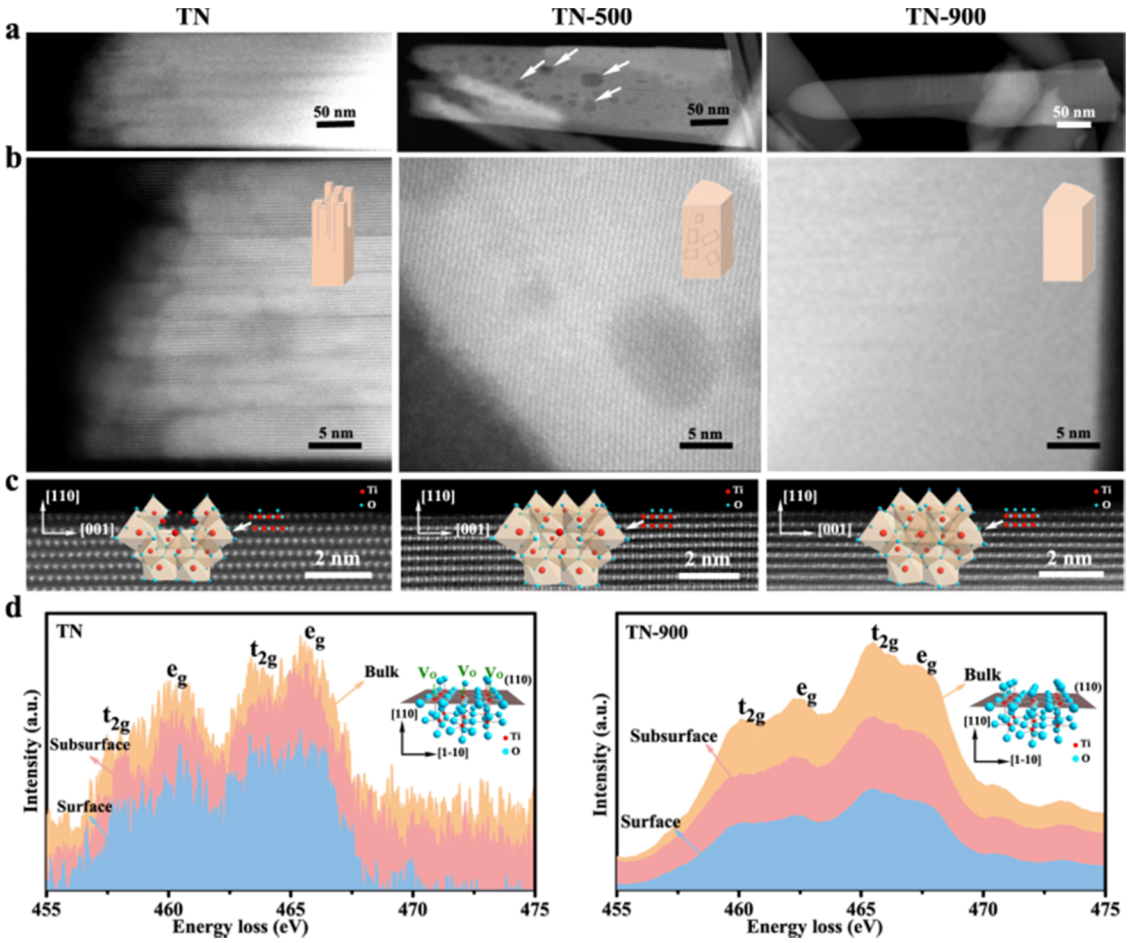


**Figure 2.** (a) TEM images of the three groups of a typical single rutile $TiO_2$ nanorod. The white arrows indicate the voids within the nanorod of the TN-500 group. (b) High-resolution TEM (HRTEM) images show the microstructures. The upper right insets are the corresponding schematic illustrations. (c) Spherical aberration (Cs) corrected TEM images show the surface atomic structures of the (110) facets taken along the ⟨1−10⟩ zone-axis direction. The insets are schematic illustrations of surface atomic structures. (d) Ti $L_{2,3}$-edge electron energy loss spectrometry (EELS) at the surface, subsurface, and bulk positions of the TN and TN-900 groups. The insets are schematic illustrations of structural models.

detected using a microplate reader (SpectraMax M5) at 562 nm.

**2.4. Statistical Analysis.** The Student's *t*-test analysis was conducted for statistical analysis. Statistical significance was considered as $*P < 0.05$, $**P < 0.01$, and $***P < 0.001$.

## 3. RESULTS AND DISCUSSION

As shown in Figure 1, the diameter of nanorods for TN, TN-500, and TN-900 was 93 ± 39, 83 ± 29, and 105 ± 21 nm, respectively, while the length of nanorods in the three groups was 489 ± 68, 463 ± 59, and 490 ± 84 nm, respectively. These results suggested that there was no obvious change in the diameter and length as well as the distribution of the nanorods before/after annealing treatment. However, as indicated by the white arrows, one can see the rough finger structure featuring the assembly of bundles of parallel nanorods in the TN group but with a relatively smooth surface of nanorods in the TN-900 group. These results were consistent with previous literature.[15] Therefore, it is reasonable to speculate that the annealing treatment must change the surface atomic structure features of the rutile nanorods.

We further carried out characterization using transmission electron microscopy (TEM) to observe the microstructures of rutile nanorods before/after annealing treatment. As shown in Figure 2a,b, the rough morphology at the rod head of the TN nanorod originated from the finger structure splitted into bundles of thin nanofibers (diameter, ∼5 nm). A high defect density of edge dislocation was therefore produced because of the internal surfaces between the nanofibers parallel to the growth direction (⟨001⟩). However, after annealing at 500 °C, the edge dislocations of the nanorod (TN-500) disappeared. Concurrently, a structural transformation occurred resulting in faceted voids of several nanometers in diameter occupied inside the nanorod but not at the surface, as indicated by the white arrows in Figure 2a. The inside voids could be removed by further increasing the annealing temperature to 900 °C (TN-900), resulting in a relatively smooth surface of the nanorod. These results were consistent with the SEM observation.

The surface atomic structures of the (110) facets of the three groups of rutile $TiO_2$ nanorods were further characterized using spherical aberration (Cs) corrected TEM taken along the ⟨1−10⟩ zone-axis direction. As shown in Figure 2c, there were abundant surface oxygen vacancy defects presented in the as-grown state of nanorods (TN) but could be removed by the annealing treatment (TN-900). We therefore further probed the surface electronic structure of the nanorods in TN and TN-900 groups using electron energy loss spectrometry (EELS) analysis. The EELS spectra of the Ti $L_{2,3}$-edge at different depths from the surface are shown in Figure 2d.


https://doi.org/10.1021/acsomega.3c02348
ACS Omega 2023, 8, 20066−20072

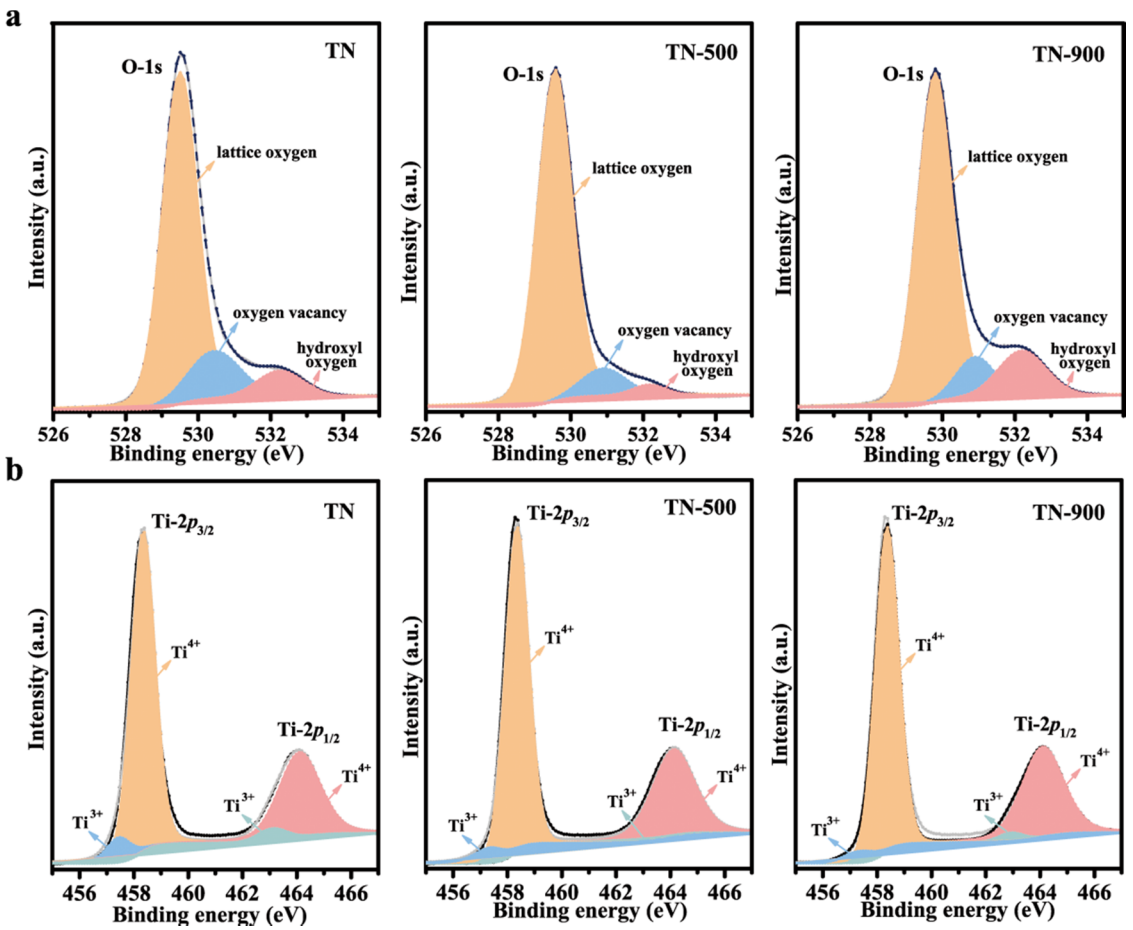


**Figure 3.** X-ray photoelectron spectroscopy (XPS) of O-1s (a) and Ti-2p (b) of the three groups of rutile $TiO_2$ nanorods.

There were mainly two doublets of the Ti $L_{2,3}$-edge resulting from the splitting of Ti 3d states into $t_{2g}$ and $e_g$ peaks of Ti $L_3$ ($2p_{3/2}$, lower energy losses) and Ti $L_2$ ($2p_{1/2}$, higher energy losses) edges.[16] The Ti $L_{2,3}$-edge of the surface position in TN did not typically split into four peaks as compared to that of TN-900 but they showed a slight shift to lower energy loss. These results demonstrated the presence of $Ti^{3+}$ defective species, suggesting the existence of surface oxygen vacancies stabilizing $Ti^{3+}$ accumulated at the surface region of TN.[17] These results were consistent with the observation of surface atomic structures.

The surface Ti valence and oxygen vacancies were further studied by using X-ray photoelectron spectroscopy (XPS). As shown in Figure 3a, the strong peak at 529.5 eV was ascribed to the O-1s spectra of lattice oxygen. The peak centered at 530.6 eV originated from the oxygen atoms of oxygen vacancy ($V_O$). And the broader peak at 532.3 eV could be ascribed to signals from the adsorption of hydroxyl groups (OH).[18] After annealing treatment, the oxygen vacancy defects were gradually eliminated from 13.82% (TN) to 6.06% (TN-900). These results were further confirmed by fitting the Ti-2p spectra. The peaks located at 458.3 and 464.0 eV could be ascribed to the Ti-$2p_{3/2}$ and Ti-$2p_{1/2}$ orbitals of $Ti^{4+}$ peaks, respectively (Figure 3b). The corresponding slightly lower shifting peaks after energy separation were derived from $Ti^{3+}$.[19] The elimination of signals from $Ti^{3+}$ valance states after annealing treatment further confirmed the attenuation of surface oxygen vacancies of rutile nanorods after annealing treatment.

To evaluate the capacity of biomineralization on three groups of rutile $TiO_2$ nanorod substrates, they were immersed in SBF to study the apatite formation.[20] Interestingly, there were aggregates composed of continuously connected leaf-like crystals on the TN and TN-500 surfaces while none were on the TN-900 surface (Figure 4a). X-ray diffraction (XRD) pattern further confirmed the HA crystal phase of the aggregates (Figure 4b). Although the underlying mechanism still remains to be uncovered, these results suggested that the capacity of biomineralization on the rutile $TiO_2$ nanorod surface was able to be controlled by the regularly used annealing treatment of $TiO_2$ nanorods.

To further evaluate the cellular mineralization behavior on various $TiO_2$ nanorods, we cultured hMSCs as the model osteoprogenitor cells on the three groups of rutile $TiO_2$ nanorod substrates (Figure 5a). As shown in Figure 5b, the intensity/number of calcium nodules (Alizarin Red area) was statistically significantly higher on TN and TN-500 than on TN-900 (Figure 5c). Although the solution environment during the cell culture process (amino acids, proteins, carbohydrates, vitamins, etc.) was much more complex than that in SBF, these results suggested that the biomineralization potential of hMSCs on the TN sample was upregulated compared to those of TN-500 and TN-900.

Biomineralization is an extremely widespread phenomenon that leads to the precipitation of organic−inorganic mineral materials.[21] The mineralization process of calcium phosphate (CaP) is considered as the core scenario in biomineralization because the carbonated calcium phosphate apatite is the


https://doi.org/10.1021/acsomega.3c02348
ACS Omega 2023, 8, 20066−20072

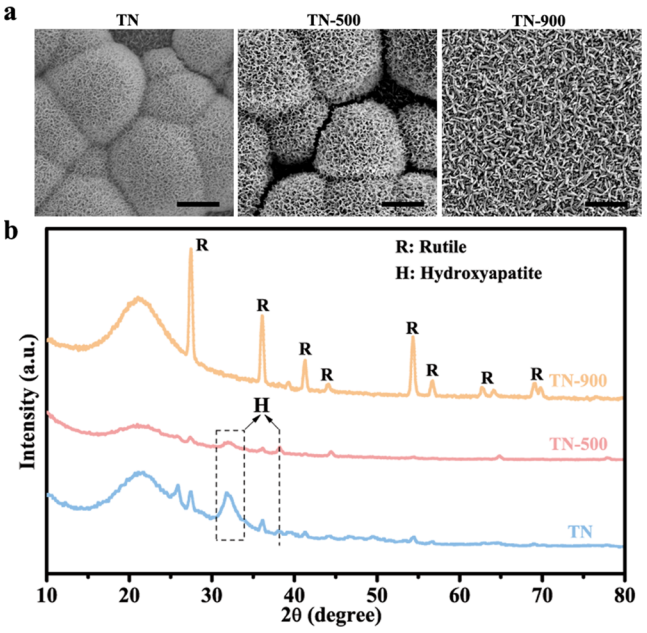


**Figure 4.** (a) SEM images and (b) X-ray diffraction (XRD) patterns of the three groups of rutile $TiO_2$ nanorod substrates after immersing in the simulated body fluid (SBF) solution. Scale bars in panel (a) are 2 $\mu$m.

essential mineral component of living organisms, such as shells, bone, teeth, etc.[22] Therefore, understanding the mechanism of CaP biomineralization on the biomaterial surface will aid in developing a novel strategy for next generation of hard tissue implant biomaterials. Although the mechanism of CaP nucleation and growth, particularly at the early stages of biomineralization, is not fully understood,[23] it is believed that the capacity to attract the adsorption of $Ca^{2+}$ ions plays a critical role in formation of CaP onto the material surface, which eventually transforms into bone-like apatite.[24] In this study, it was reasonable to further speculate that the surface oxygen vacancy defects of rutile nanorods were beneficial for the adsorption of $Ca^{2+}$, facilitating the heterogeneous nucleation of HA onto rutile nanorods. For example, Sasahara et al. reported that CaP particles were able to precipitate on the air-annealed $TiO_2$ (110) surface but were suppressed once the substrate was preannealed in $O_2$ before immersion in Hanks' balanced salt solution (HBSS) because of the transformation of the amorphous phase in the topmost layer to the rutile phase, which resulted in the failing lattice mismatch for epitaxial growth of brushite.[25] Transformation of the amorphous phase in the topmost layer to the rutile phase after annealing in $O_2$ suggested the elimination of surface oxygen vacancies. Previous studies also indicated that hydrothermally grown rutile $TiO_2$ nanowires were intrinsically full of oxygen vacancy defects, which were significantly reduced after annealing at 500 °C in air, as vacancy condensation into internal voids occurred during the heat treatment.[17,26] Our TEM results of TN-500 (Figure 4a) further confirmed this conclusion. Moreover, our results have shown that when the annealed temperature increased to 900 °C, the vacancies further vanished due to the oxygen atmosphere during the heat treatment. It was suggested by the thermodynamically driven oxidation of $Ti^{3+}$ into $Ti^{4+}$ during heat treatment, compensating the oxygen vacancies.[27] These results suggested that surface oxygen vacancy defects of rutile nanorods could be controlled by simple annealing treatment in air atmosphere. Recently, Surmeneva et al. also reported that heat treatment in vacuum at a relatively low temperature, such as 700 °C, also had a dramatic influence on the surface microstructure of oxides, suggesting that the atmospheric annealing and temperature might be the coupling parameters.[28] It was noteworthy that the roughness of the head of nanorods might play a role in aggregation of HA and mineralization of hMSCs.[29,30] Indeed, our results showed the roughness of the head of nanorods varied significantly after annealing treatment (Figure 1). However, the area of the nanorod head was relatively small and cellular filopodia were more likely to anchor the columnar surface of the nanorods.[31] We therefore speculated that surface

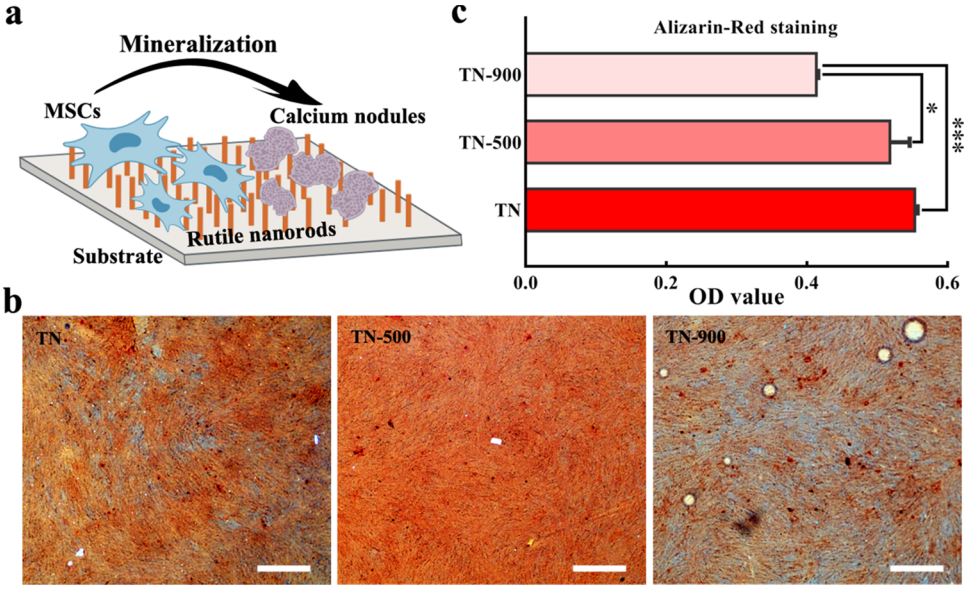


**Figure 5.** (a) Schematic illustration of hMSC mineralization on rutile $TiO_2$ nanorod substrates. (b) Images of mineralization capacity of hMSCs on three groups of rutile $TiO_2$ nanorod substrates evaluated by Alizarin Red staining and their corresponding quantitative analysis (c). Scale bars in panel (c) are 500 $\mu$m.



https://doi.org/10.1021/acsomega.3c02348
ACS Omega 2023, 8, 20066−20072

oxygen vacancies of rutile nanorods played a key role during the aggregation of HA and mineralization of hMSCs. In terms of the possible effects of crystalline phases, such as rutile or anatase, we considered that the rutile phase was the thermodynamic stable phase, while the anatase phase would change into rutile one during the heat treatment. It was therefore difficult to identify the role of phase or surface feature on biomineralization if we selected the anatase phase in this work. However, we believed that the key role of surface oxygen vacancies on biomineralization would be a general phenomenon, regardless of the crystal phase.

Some literature studies also suggested that the surface hydroxyl group was an important candidate in CaP deposition and osteogenic differentiation of osteoprogenitor cells.[32−34] However, the results in Figure 5a indicated the content of the surface hydroxyl group in TN-900 was upregulated compared to that of TN. These results suggested that not all of the types of hydroxyl groups helped to attract $Ca^{2+}$ adsorption.[9] Moreover, surface oxygen vacancy defects could behave as adsorption and active sites for generation of hydroxyl groups.[10] In terms of the upregulated mineralization of hMSCs on $TiO_2$ nanorods of the TN group, recent studies have shown that the osteogenesis of osteoprogenitor cells could be triggered by extracellular $Ca^{2+}$ through type L voltage-gated calcium channels.[35] Some other literature studies also demonstrated that $PO_4^{3-}$ ions were predominantly adsorbed on the oxygen-vacancy-rich nitrogen-doped $TiO_2$ soaked in SBF, followed by $Ca^{2+}$ ions.[36] The mechanism of biomineralization on the material surface is complex and may involve multiple steps. First, the adsorbed ions, proteins, or other biomolecules act as templates to form the small clusters as the mineral nuclei. This step is dominated by a combination of surface feature factors, such as roughness, porosity, surface charge, wettability, etc. Then, the mineral nuclei grow through the process of ion accretion, in which ions in the surrounding solution are incorporated into the growing mineral structure. This mineral growth process is controlled by the concentration of ions, the surface chemistry of substrate, as well as other biomolecules in the solution. For example, a negatively charged surface can attract positively charged biomolecules and ions, such as $Ca^{2+}$, leading to enhanced mineralization. A rough surface with distinct topography is able to provide more binding sites for biomolecules and ions and create more pockets and crevices for mineral nuclei formation and growth. It is worth noting that not only oxygen vacancies but also roughness, porosity, surface chemistry, etc., have simultaneously been changed by the annealing treatment in this work. It is hard to decouple them as a single factor in this system currently. All in all, the details of the heterogeneous nucleation and growth of HA by triggering the accumulation of $Ca^{2+}$ or $PO_4^{3-}$ ions on the oxygen vacancy defective surface still need to be further studied.

## 4. CONCLUSIONS

In summary, we demonstrate that the surface oxygen vacancy defects of rutile nanorods could be gradually eliminated by the regularly used annealing treatment, which restrained the heterogeneous nucleation of hydroxyapatite (HA) onto rutile nanorods in simulated body fluids (SBFs) and the mineralization of hMSCs. Moreover, the concentration and feature of surface oxygen vacancy defects of rutile nanorods are dependent on the annealing temperature. This study emphasizes the importance of the subtle changes of surface features down to the atomic scale of oxidic biomaterials during the commonly used processing and therefore provides new insights into the fundamental understanding of biomineralization on the biomaterial surface and will have a profound impact on further designing novel hard tissue implant biomaterials.

## AUTHOR INFORMATION


### Corresponding Author

**Tong Wu** − *Guangdian Metrology & Testing (Hangzhou) Co., Ltd., Hangzhou 310018 Zhejiang, China;* orcid.org/0009-0003-6984-7269; Email: wutong@grgtest.com

### Authors

**Yanwen Yu** − *First People's Hospital of Linping District, Hangzhou 311100 Zhejiang, China*

**Lingqing Dong** − *Stomatology Hospital, School of Stomatology, Zhejiang University School of Medicine, Zhejiang Province Clinical Research Center for Oral Diseases, Key Laboratory of Oral Biomedical Research of Zhejiang Province, Cancer Center of Zhejiang University, Hangzhou 310006, China;* orcid.org/0000-0002-2203-3212

Complete contact information is available at: https://pubs.acs.org/10.1021/acsomega.3c02348


### Notes

The authors declare no competing financial interest.

## ACKNOWLEDGMENTS

This work was supported by the Key Laboratory of Oral Biomedical Research of Zhejiang Province Foundation (2021M003). The author is also grateful to Dr. Guohui Shou and Dr. Wentao Yuan from the School of Materials Science and Engineering, Zhejiang University, and Dr. Xiaowen Yu from Stomatology Hospital, School of Stomatology, Zhejiang University School of Medicine, for their technical support and constructive discussion.

## REFERENCES


(1) Wu, S.; Weng, Z.; Liu, X.; Yeung, K. W. K.; Chu, P. K. Functionalized $TiO_2$ Based Nanomaterials for Biomedical Applications. *Adv. Funct. Mater.* **2014**, *24*, 5464−5481.

(2) Kokubo, T. Apatite formation on surfaces of ceramics, metals and polymers in body environment. *Acta Mater.* **1998**, *46*, 2519−2527.

(3) Wang, N.; Li, H.; Lue, W.; Li, J.; Wang, J.; Zhang, Z.; Liu, Y. Effects of $TiO_2$ nanotubes with different diameters on gene expression and osseointegration of implants in minipigs. *Biomaterials* **2011**, *32*, 6900−6911.

(4) Zhou, J.; Li, B.; Han, Y. F-doped $TiO_2$ microporous coating on titanium with enhanced antibacterial and osteogenic activities. *Sci. Rep.* **2018**, *8*, No. 17858.

(5) Shrestha, S.; Mao, Z.; Fedutik, Y.; Gao, C. Influence of titanium dioxide nanorods with different surface chemistry on the differentiation of rat bone marrow mesenchymal stem cells. *J. Mater. Chem. B* **2016**, *4*, 6955−6966.

(6) Gower, L. B. Biomimetic Model Systems for Investigating the Amorphous Precursor Pathway and Its Role in Biomineralization. *Chem. Rev.* **2008**, *108*, 4551−4627.

(7) Wang, S.; Yang, Y.; Wang, R.; Kong, X.; Wang, X. Mineralization of calcium phosphate controlled by biomimetic self-assembled peptide monolayers via surface electrostatic potentials. *Bioact. Mater.* **2020**, *5*, 387−397.

(8) Wang, L.; Nancollas, G. H. Calcium Orthophosphates: Crystallization and Dissolution. *Chem. Rev.* **2008**, *108*, 4628−4669.




https://doi.org/10.1021/acsomega.3c02348
*ACS Omega* 2023, 8, 20066−20072

(9) Lu, X.; Zhang, H.-p.; Leng, Y.; Fang, L.; Qu, S.; Feng, B.; Weng, J.; Huang, N. The effects of hydroxyl groups on Ca adsorption on rutile surfaces: a first-principles study. *J. Mater. Sci.: Mater. Med.* **2010**, *21*, 1−10.
(10) Wu, S.; Xiong, J.; Sun, J.; Hood, Z. D.; Zeng, W.; Yang, Z.; Gu, L.; Zhang, X.; Yang, S.-Z. Hydroxyl-Dependent Evolution of Oxygen Vacancies Enables the Regeneration of BiOCl Photocatalyst. *ACS Appl. Mater. Interfaces* **2017**, *9*, 16620−16626.
(11) Zhu, J.; Farmer, J. A.; Ruzycki, N.; Xu, L.; Campbell, C. T.; Henkelman, G. Calcium adsorption on MgO(100): Energetics, structure, and role of defects. *J. Am. Chem. Soc.* **2008**, *130*, 2314−2322.
(12) Huang, L.; Shen, J.; Dong, L.; Chen, Q. Simultaneous acceleration of osteogenesis and angiogenesis by surface oxygen vacancies of rutile nanorods. *Colloids Surf., B* **2022**, *212*, No. 112348.
(13) Tang, D.; Cheng, K.; Weng, W. J.; Song, C. L.; Du, P. Y.; Shen, G.; Han, G. R. $TiO_2$ nanorod films grown on Si wafers by a nanodot-assisted hydrothermal growth. *Thin Solid Films* **2011**, *519*, 7644−7649.
(14) Zhou, Y.; Dong, L. Q.; Liu, C.; Lin, Y. H.; Yu, M. F.; Ma, L.; Zhang, B.; Cheng, K.; Weng, W. J.; Wang, H. M. Engineering prevascularized composite cell sheet by light-induced cell sheet technology. *RSC Adv.* **2017**, *7*, 32468−32477.
(15) Wisnet, A.; Betzler, S. B.; Zucker, R. V.; Dorman, J. A.; Wagatha, P.; Matich, S.; Okunishi, E.; Schmidt-Mende, L.; Scheu, C. Model for Hydrothermal Growth of Rutile Wires and the Associated Development of Defect Structures. *Cryst. Growth Des.* **2014**, *14*, 4658−4663.
(16) Folger, A.; Ebbinghaus, P.; Erbe, A.; Scheu, C. Role of Vacancy Condensation in the Formation of Voids in Rutile $TiO_2$ Nanowires. *ACS Appl. Mater. Interfaces* **2017**, *9*, 13471−13479.
(17) Lim, J.; Kim, S.-H.; Armengol, R. A.; Kasian, O.; Choi, P.-P.; Stephenson, L. T.; Gault, B.; Scheu, C. Atomic-Scale Mapping of Impurities in Partially Reduced Hollow $TiO_2$ Nanowires. *Angew. Chem., Int. Ed.* **2020**, *59*, 5651−5655.
(18) Ishfaq, M.; Khan, M. R.; Bhopal, M. F.; Nasim, F.; Ali, A.; Bhatti, A. S.; Ahmed, I.; Bhardwaj, S.; Cepek, C. 1.5 MeV proton irradiation effects on electrical and structural properties of $TiO_2$/n-Si interface. *J. Appl. Phys.* **2014**, *115*, No. 174506.
(19) Xiao, F.; Zhou, W.; Sun, B.; Li, H.; Qiao, P.; Ren, L.; Zhao, X.; Fu, H. Engineering oxygen vacancy on rutile $TiO_2$ for efficient electron-hole separation and high solar-driven photocatalytic hydrogen evolution. *Sci. China Mater.* **2018**, *61*, 822−830.
(20) Kokubo, T.; Takadama, H. How useful is SBF in predicting in vivo bone bioactivity? *Biomaterials* **2006**, *27*, 2907−2915.
(21) Cano, M.; Giner-Casares, J. J. Biomineralization at fluid interfaces. *Adv. Colloid Interface Sci.* **2020**, *286*, No. 102313.
(22) Wang, X.; Yang, J.; Andrei, C. M.; Soleymani, L.; Grandfield, K. Biomineralization of calcium phosphate revealed by in situ liquid-phase electron microscopy. *Commun. Chem.* **2018**, *1*, No. 80.
(23) He, K.; Sawczyk, M.; Liu, C.; Yuan, Y.; Song, B.; Deivanayagam, R.; Nie, A.; Hu, X.; Dravid, V. P.; Lu, J.; Sukotjo, C.; Lu, Y.-p.; Kral, P.; Shokuhfar, T.; Shahbazian-Yassar, R. Revealing nanoscale mineralization pathways of hydroxyapatite using in situ liquid cell transmission electron microscopy. *Sci. Adv.* **2020**, *6*, No. eaaz7524.
(24) Barradas, A. M. C.; Monticone, V.; Hulsman, M.; Danoux, C.; Fernandes, H.; Birgani, Z. T.; Barrere-de Groot, F.; Yuan, H. P.; Reinders, M.; Habibovic, P.; van Blitterswijk, C.; de Boer, J. Molecular mechanisms of biomaterial-driven osteogenic differentiation in human mesenchymal stromal cells. *Integr. Biol.* **2013**, *5*, 920−931.
(25) Sasahara, A.; Murakami, T.; Tomitori, M. Dependence of calcium phosphate formation on nanostructure of rutile $TiO_2$(110) surfaces. *Jpn. J. Appl. Phys.* **2018**, *57*, No. 115501.
(26) Folger, A.; Kalb, J.; Schmidt-Mende, L.; Scheu, C. Tuning the Electronic Conductivity in Hydrothermally Grown Rutile $TiO_2$ Nanowires: Effect of Heat Treatment in Different Environments. *Nanomaterials* **2017**, *7*, No. 289.
(27) Padmini, M.; Balaganapathi, T.; Thilakan, P. Rutile-$TiO_2$: Post heat treatment and its influence on the photocatalytic degradation of MB dye. *Ceram. Int.* **2022**, *48*, 16685−16694.
(28) Surmeneva, M.; Prosolov, K.; Glukhov, I.; Grubova, I.; Botvin, V.; Surmenev, R.; Sharkeev, Y. Effects of annealing in vacuum on the microstructure of silicon-containing calcium phosphate films deposited on a ZrNb alloy by radio-frequency magnetron sputtering. *Vacuum* **2023**, *212*, No. 112028.
(29) Chen, X. B.; Nouri, A.; Li, Y. C.; Lin, J. G.; Hodgson, P. D.; Wen, C. Effect of surface roughness of Ti, Zr, and TiZr on apatite precipitation from simulated body fluid. *Biotechnol. Bioeng.* **2008**, *101*, 378−387.
(30) Hou, Y.; Xie, W.; Yu, L.; Camacho, L. C.; Nie, C.; Zhang, M.; Haag, R.; Wei, Q. Surface Roughness Gradients Reveal Topography-Specific Mechanosensitive Responses in Human Mesenchymal Stem Cells. *Small* **2020**, *16*, No. 1905422.
(31) Cheng, K.; Yu, M. F.; Liu, Y.; Ge, F.; Lin, J.; Weng, W. J.; Wang, H. M. Influence of integration of $TiO_2$ nanorods into its nanodot films on pre-osteoblast cell responses. *Colloids Surf., B* **2015**, *126*, 387−393.
(32) Turkan, U.; Guden, M. The effect of surface treatment on CaP deposition of Ti6Al4V open cell foams in SBF solution. *Ceram. Int.* **2010**, *36*, 1805−1816.
(33) Kim, H. M.; Miyaji, F.; Kokubo, T.; Nakamura, T. Effect of heat treatment on apatite-forming ability of Ti metal induced by alkali treatment. *J. Mater. Sci.: Mater. Med.* **1997**, *8*, 341−347.
(34) Yu, M. F.; Gong, J. X.; Zhou, Y.; Dong, L. Q.; Lin, Y. H.; Ma, L.; Weng, W. J.; Cheng, K.; Wang, H. M. Surface hydroxyl groups regulate the osteogenic differentiation of mesenchymal stem cells on titanium and tantalum metals. *J. Mater. Chem. B* **2017**, *5*, 3955−3963.
(35) Barradas, A. M. C.; Fernandes, H. A. M.; Groen, N.; Chai, Y. C.; Schrooten, J.; van de Peppel, J.; van Leeuwen, J.; van Blitterswijk, C. A.; de Boer, J. A calcium-induced signaling cascade leading to osteogenic differentiation of human bone marrow-derived mesenchymal stromal cells. *Biomaterials* **2012**, *33*, 3205−3215.
(36) Hashimoto, M.; Hayashi, K.; Kitaoka, S. Enhanced apatite formation on Ti metal heated in $PO_2$-controlled nitrogen atmosphere. *Mater. Sci. Eng.: C* **2013**, *33*, 4155−4159.


https://doi.org/10.1021/acsomega.3c02348
*ACS Omega* 2023, 8, 20066−20072